Chapter 7
Experimental Determination of Ferberite Solubility in the KCl–HCl–H_2O System at 400–500 °C and 20–100 MPa

Alexander F. Redkin and Gary L. Cygan

Abstract The solubility of ferberite, $FeWO_4$ was studied at 400–500 °C, pressures of 20, 25, 40, 50 and 100 MPa, oxygen fugacity corresponding to the Ni–NiO, Fe_3O_4–Fe_2O_3 buffers, in 0.7 ÷ 8.9 *m*KCl solutions and acidity controlled by quartz-microcline-muscovite buffer assemblage. The parameters of the experiments cover both the field of homogeneous solutions and the region of immiscibility in the KCl–H_2O system. The total W concentration depends upon *m*Cl, *T* and fO_2 in the system and range from $1 \cdot 10^{-4}$–0.05 mol kg^{-1} in 0.7 *m*KCl to 0.01–0.15 in 8.9 *m*KCl. The results suggest a large bulk solubility in the dense, salt-rich phase of the two-phase fluid. Ferberite dissolution in KCl solutions under pH and fO_2 buffered conditions at 400–500 °C proceeds congruently as well as incongruently with accompanying potassium tungsten bronzes formation, K_xWO_3, (x = 0.2–0.3). Thermodynamic calculations performed for a homogeneous solution at $P = 100$ MPa indicate that the predominant aqueous species of tungsten in KCl–HCl solutions at $fO_2 = fO_2$(Ni–NiO) may be W(V, VI) species: WO_3^-, HWO_4^-, $H_2W_2O_7^-$ at 500 °C and HWO_4^-, $W_5O_{16}^{3-}$ at 400 °C. Application of the extended $FeWO_4$ solubility model to natural systems suggest that deposition of tungsten from ore-bearing solutions is due to interaction with wall rocks containing feldspars, and iron oxides together with decreasing temperatures. In the magnetite bearing system, the equilibrium tungsten concentration does not exceed $2 \cdot 10^{-5}$ mol kg^{-1} at temperatures of 400 °C.

Keywords Ferberite · Potassium tungstate bronze · Solubility · Buffered system · Homogenous solution · Immiscibility region · Tungsten species

7.1 Introduction

Wolframite, $(Fe, Mn)^{+2}WO_4$, as well as its end members ferberite, $FeWO_4$, and huebnerite, $MnWO_4$, are the main ore minerals associated with hydrothermal deposits of

A. F. Redkin (✉)
Institute of Experimental Mineralogy, Russian Academy of Sciences, Moscow, Russia 142432
e-mail: redkin@iem.ac.ru

G. L. Cygan
U.S. Environmental Protection Agency, Chicago, IL 60604, USA

Y. Litvin and O. Safonov (eds.), *Advances in Experimental and Genetic Mineralogy*, Springer Mineralogy, https://doi.org/10.1007/978-3-030-42859-4_7

tungsten related to the metasomatic processes of granite greisenization and albitization. Tungsten ore deposition usually occurs late in the paragenetic sequence and is typically located in the apical segments of massifs. Mineralization typically occurs at depths equated with the range of 100–150 m. Temperature conditions of ore formation are estimated to be in the interval 300–540 °C (Smirnov et al. 1981). According to mineral-geochemical investigations ore deposition took place in several stages, typically as part of the post-greisen stage of development. The greisen metasomatic process created conditions appropriate for leaching W and other ore elements (e.g., Fe, U, REE) from the surrounding rocks interacting with the hydrothermal solutions. The analysis of gas-liquid inclusions in quartz from greisen of different generations (Ivanova et al. 1986) indicate wolframite deposits were formed under the influence of solutions containing high concentrations of salts (dominantly NaCl, KCl), carbon dioxide and rich in fluorides. Hydrothermal solutions containing tungsten leached iron from the host rock, effectively bleaching the host rock. It appears that the calcium content in these hydrothermal solutions is not critical since we observe sheelite ($CaWO_4$) mineralization principally associated with skarns. Tungsten ore deposition in these, high-temperature, high-concentration salt solutions occurred during the greisen stage of the hydrothermal process. The hydrothermal solution had the same acidity as that of the solutions forming quartz-topaz and quartz-mica (muscovite) greisens. For these reasons, a study of ferberite solubility in highly concentrated salt solutions, particularly the two-phase region of aqueous-salt fluids, under buffered conditions is a principal problem in tungsten geochemistry. In addition, investigations into the effect of pressure on the solubility of ore minerals is also of considerable interest since it has been demonstrated by Hemley et al. (1986, 1992), Malinin and Kurovskaya (1996) that pressure decreases can increase metal solubility in acid-buffered systems.

7.2 Experimental Procedures

Experiments were performed at 400–500 °C and pressures of 20, 25, 40, 50 and 100 MPa using large volume hydrothermal pressure vessels (30 mm internal diameter × 200 mm long): cold-seal pressure vessels (Tuttle bombs) and a pinch-off vessel (Ivanov et al. 1994). A drawing of the Pinch-off device in thin-wall capsule of gems is represented in Fig. 7.1a, b. The experimental charge in the welded capsule is positioned in the clamping mechanism and placed between the two halves of the prop above the connector. The clamp location on the capsule may be moved so that the ratio of the separated, or "pinched-off" capsule may be varied (Fig. 7.1a). This pinch-off mechanism is operated by way of a hydraulic push of the rod that moves the pinching tool upwards causing the pincering effect to occur. The pincer consists of two identical halves with a conical external surface, specially designed internal longitudinal hollows and transverse connectors. Crushing and collapsing of the capsule does not occur because of these longitudinal grooves and connectors. The walls of the capsule are pressed tightly enough that a weld occurs at the pinch point

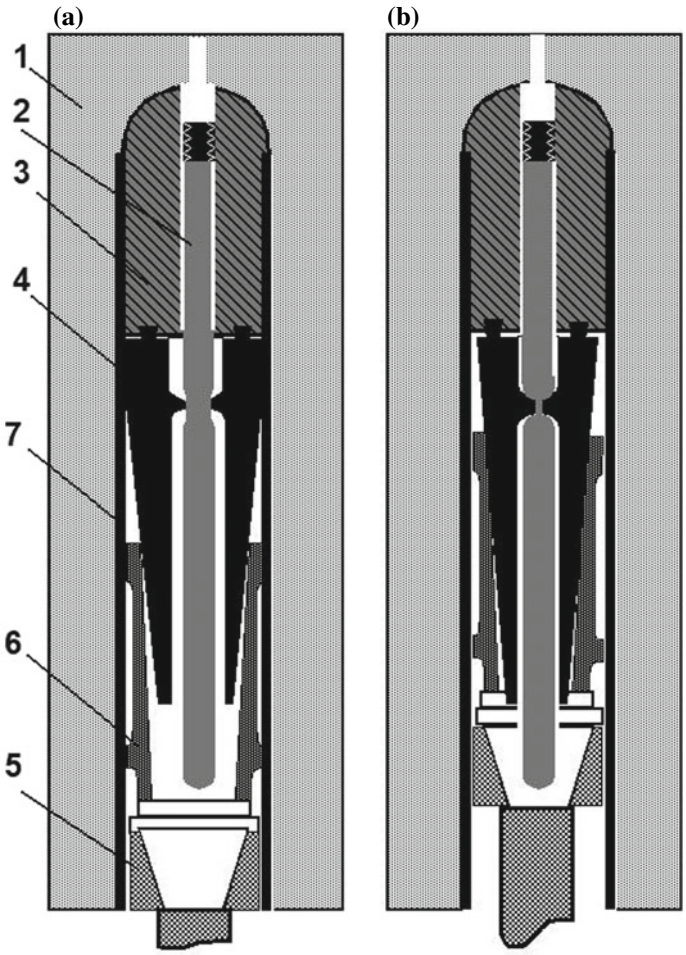

Fig. 7.1 Schematic showing the pinch-off vessel used for separation of media under hydrothermal conditions: **a** initial state; **b** after the separator with the one connector has been activated. Details of the device: 1—Ni-alloy reactor, 2—capsule, 3—stop holder (two details), 4—separator or capsule clamp (two details), 5—movable socket rod, 6—movable sleeve, 7—tube

(Fig. 7.1b). The hot spot of the furnace was measured and found to have a thermal gradient of 2–3 °C over 12 cm. The capsule pinching was done after the necessary time required for establishing equilibrium. The pinch-off vessel was used to refine KCl concentration in brine at 500 °C and pressure of 40 and 50 MPa.

Using large volume vessel (cold seals Tuttle bomb), four experiments on ferberite solubility were run simultaneously. Temperature was regulated using a high-precision controller using chromel-alumel thermocouples between the experimental capsules. The thermocouple uncertainty is ±2–3 °C. Experiments at pressures of 20–50 MPa were set using a Burdon manometer for pressures of up to 60 MPa and an uncertainty

of ±0.2 MPa. Experiments conducted at 100 MPa used a 2500-style manometer with an accuracy of ±15 MPa. Experimental run times were from 14 to 30 days, depending upon *P* and *T*, though previous studies in similar systems containing the ore minerals SnO_2, UO_2, $CaWO_4$, indicate equilibrium with the solutions is approached in several hours to less than 7 days (Dadze et al. 1981; Kovalenko et al. 1986; Redkin et al. 1989; Malinin and Kurovskaya 1996).

Study of ferberite solubility in aqueous-salt KCl–HCl solutions was made in platinum capsules, 60–90 mm long × 7–8 mm diameter. The starting solutions for the experiments were made from commercial reagents of high-purity KCl, HCl and doubly-distilled water. Pressures and starting KCl compositions were chosen such that the experiments would be in the two-phase region (Fig. 7.2a, b). At 500 °C and

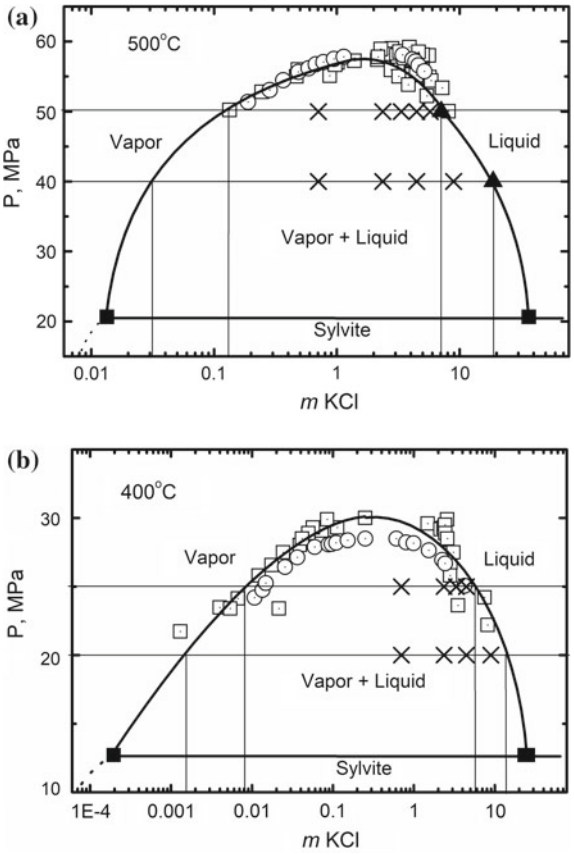

Fig. 7.2 Vapor and liquid compositions along the 500 (**a**) and 400 °C (**b**) isothermal coexistence curves for the KCl–H_2O system. Solid square symbols for three-phase (sylvite-liquid-vapor) by Hovey et al. (1990). For two-phase region: dotted square by Cygan et al. (1994), dotted round by Shmulovich et al. (1995), solid triangles represent our data obtained using the pinch-off device. The initial *m*KCl values used in the runs on ferberite solubility are shown by "X"

a pressure of 40 and 50 MPa, 5, 15, 25 and 20 or 30 wt% solutions of KCl were used (Fig. 7.2a), and at 400 °C 20, 25 and 100 MPa, 5, 15, 25 and 40 wt% of KCl were used (Fig. 7.2b). The initial solutions also contained HCl of 0.01 and 0.1 or 0.001 mol/kg H_2O. Varying starting *m*KCl/*m*HCl ratios made it possible to approach equilibrium in the QMM buffer system from both sides as was done by Hemley (1959).

Ferberite starting material was synthesized through recrystallization of a mixture of FeO and WO_3 in a solution of 30 wt% LiCl in gold capsules. The ratio of the aqueous solution to the solid mixture was about 2:1 by weight. This mixture was then reacted at 500 °C and 100 MPa (Klevtsov et al. 1970) for 14 days. This produced grain sizes of 5–10 μm in diameter, and subsequent recrystallization in the same solution and T at $P = 40$ MPa for 14 days yielded grains diameters of 15–25 μm. X-ray diffraction scans of synthetic ferberite correspond to the standard sample 27–256 (PDF 1980), while microprobe analyses indicate the composition corresponds to the stoichiometric formula of ferberite, $FeWO_4$. Fourier transform infrared (FTIR) spectrum of the synthetic ferberite, depicted in Fig. 7.3, also indicates that the synthesized product is pure and complete conversion of FeO and WO_3 has occurred.

The initial solid charge consisted of a mixture of 20 mg of ferberite with 60 mg of the alumina-silicate buffer, quartz (SiO_2)-microcline ($KAlSi_3O_8$)-muscovite ($KAl_3Si_3O_{10}(OH)_2$)-(QMM). The initial Na_2O concentration of a natural pegmatitic

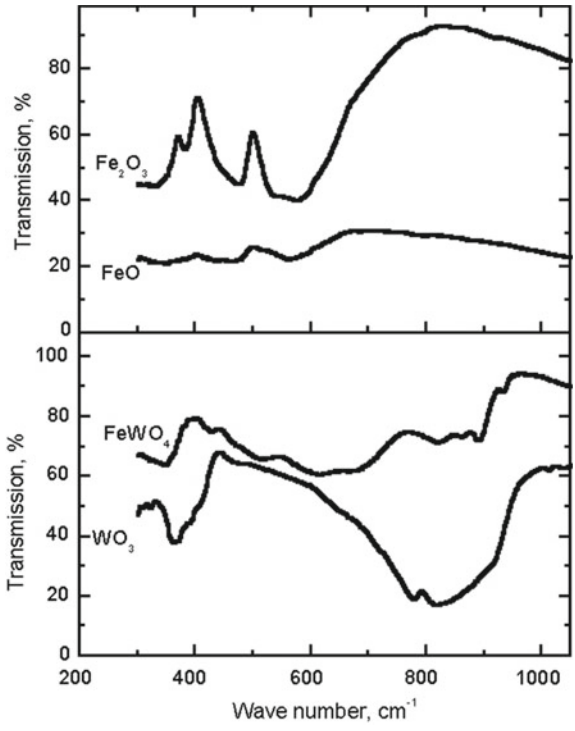

Fig. 7.3 Infra-red spectra of synthetic ferberite and the starting compounds FeO and WO_3 used in the ferberite synthesis

microcline (as Mic phase) was decreased through exposure to molten KCl. The exchange yielded a microcline composition of (in wt%) SiO_2-65.59, Al_2O_3-17.72, K_2O-16.44, FeO < 0.12, TiO_2 < 0.06, Na_2O, MnO, MgO, Cr_2O_3, CaO < 0.02. Pegmatic $2M_1$ muscovite was processed by rubbing plates of the pure natural mineral (composition (in wt%) SiO_2-47.79, TiO_2-0.64, Al_2O_3-32.46, Fe_2O_3-3.17, MnO-0.13, MgO-1.317, CaO-0.070, Na_2O-0.61, K_2O-10.77, H_2O + 2.52, F_2 < 0.04). The muscovite was sieved to 20–300 μm and then purified in dilute HCl. Before crushing in an agate mortar, synthetic quartz was heated briefly in a furnace to 700 °C and quenched in pure water to form fractures. The QMM buffer is required in this study to provide a constant KCl/HCl ratio in the aqueous phase to control the system's acidity through the following reaction:

$$1.5\text{Mic} + \text{HCl}_{(\text{aq})} = 3\text{Qtz} + 0.5\text{Ms} + \text{KCl}_{(\text{aq})} \tag{7.1}$$

In the two-phase region of the KCl–H_2O system, the QMM buffer will provide constant concentrations of KCl and HCl in each phase at a given T and P. A change in the initial KCl concentration alters the relative masses or volumes of the L and V phases, but not the KCl and HCl concentrations (Cygan et al. 1994).

Oxygen fugacity in the experiments was controlled using the nickel-bunsenite (NNO, $fO_2 = 10^{-17.70}$ at 500 °C and $10^{-22.42}$ Pa at 400 °C) and hematite-magnetite oxygen buffers (HM, $fO_2 = 10^{-13.63}$ Pa at 500 °C). The buffers consisted of approximately a 1:1 ratio of fine-crystalline metallic nickel and bunsenite or synthetic magnetite and commercial hematite, a total amount of 3–4 g was placed into the Ni-alloy container. The presence of Ni and Fe_3O_4 in the reaction mixture after the runs was checked by magnet.

Platinum capsules with the charge of solid phases (80 mg) and solution (0.4 ml) were assembled. The air above the charge was removed by blowing pure argon through the capsule before welding. We feel this contributed to a more rapid attainment of equilibrium fO_2.

The charges were quenched to room temperature using an air-water mixture for 7–10 min. The capsules were recovered, dried and weighed to check for the integrity of the capsule seal. Capsules showing less than ±5 mg change in weight were considered valid runs. The capsules were opened and the solutions and the charge were washed into plastic test-tubes using approximately a 20-fold volume of doubly-distilled water. The dilution of the recovered aqueous solution was determined by weighing the washed material to an accuracy of ±0.03 mg. These solutions were then centrifuged at a velocity of 5000–6000 rpm for 2–3 min. An aliquot of pure solution for chemical analysis was removed. The recovered solid materials were washed with doubly-distilled water and then centrifuged and dried in ceramic cups at 100–120 °C.

The transparent, colorless solutions were subjected to spectrophotometric analysis for tungsten using a Spekol-11 (Germany) and the bromopyrogallol red technique (Andreeva et al. 1992). For iron we used the ortho-phenantroline and α, α-dipyridill technique (Marczenko 1976), and for SiO_2, mainly the molybdate yellow method (Teleshova 1973). Aqueous Al analyses were performed using an atomic absorption

spectrometer (Perkin-Elmer model 403). All our attempts to use spectrophotometric analysis for Al using the antrazochrom technique (Basargin et al. 1976) were unsuccessful due to the strong interfering effect that high W concentrations had on measurements. The analytical error for Fe is estimated to be <5%, for W and SiO_2 < 10%, and for Al < 30%. Solid charge products were subjected to a quantitative microprobe analysis using a Camebax MBX at $E_o = 15$ keV, the size of beam of electrons Ø = 1–2 μm and X-ray diffraction investigations using a DRON-2 (made in Russia) with Cu-Kα.

7.3 Solubility-Salt Concentration Correlation

The solubility of a congruently-dissolving mineral in the two-phase region at constant pressure and acidity of the V and L phases can be described by the equation

$$S_{total} = S^V \cdot X_V + S^L \cdot X_L = S^V + X_L \cdot \left(S^L - S^V\right), \tag{7.2}$$

where S_{total} is a total mineral solubility in the two-phase region (wt%), S^L and S^V are the mineral solubility in L (high-density) and V (low-density) phases, and X_L and X_V are the mass fractions of L and V. Equation (7.2) represents a general expression of the lever rule for phases in equilibrium, and describes the distribution of KCl as well

$$C^T_{salt} = C^L_{salt} \cdot X_L + C^V_{salt} \cdot X_V,$$

where C^T_{salt}, C^L_{salt}, and C^V_{salt} are the total concentration of salt and concentrations of salt in the coexisting L and V phases in wt%, respectively. It follows,

$$X_L = \left(C^T_{salt} - C^V_{salt}\right)/\left(C^L_{salt} - C^V_{salt}\right). \tag{7.3}$$

Replacing X_L in (7.2) by (7.3) we get the expression where mineral solubility depends linearly on total salt concentration, C^T_{salt}, whereas S^V, S^L, C^L_{salt}, and C^V_{salt} are constant:

$$S_{total} = S^V + \left(S^L - S^V\right) \cdot \left(C^T_{salt} - C^V_{salt}\right)/\left(C^L_{salt} - C^V_{salt}\right), \tag{7.4}$$

and $S_{total} = S^V$ at $C^T_{salt} = C^V_{salt}$ and $S_{total} = S^L$ at $C^T_{salt} = C^L_{salt}$. It is clear that in the two-phase region, we can speak about solubility of a compound either in a liquid or in the vapor phase. However, the value S_{total} itself represents an apparent solubility, that is, a total solubility obtained after fluid homogenization after quench. Nevertheless, these apparent mineral solubility data may be described by using a linear function of the total salt concentration in a fluid.

7.4 Results and Discussions

7.4.1 Solutions After the Runs

Experimental results are represented in Table 7.1 and Fig. 7.4a, b. Quench pH values of parallel experiments, that is, experiments made at the same initial concentration of KCl but different *m*HCl (0.1 and 0.01), are quite similar indicating the acidic-alkaline equilibrium between the QMM buffer and KCl–HCl–H_2O solution is operating. The divergence in *m*HCl values of some runs, especially those conducted in 40 wt% KCl starting solutions (Fig. 7.5), may be related to the effect of high concentrations of Fe and W on the quenched pH value (*m*HCl). Total W and Fe concentrations are a function of the *m*KCl and the initial *m*HCl. These varied from $1 \cdot 10^{-4}$–0.05 in 0.7 *m*KCl starting solution experiments to 0.01–0.15 m in 8.9 *m*KCl (see Fig. 7.4a). Incongruent dissolution of ferberite is indicated by the fact that *m*W was consistently not equal to *m*Fe in the analyzed solutions. Despite the significant concentrations of W and Fe (0.02–0.15 mol kg^{-1}) the quenched solutions were acidic, transparent, and colorless (or light blue (Busev et al. 1976)) suggesting that iron in the solutions was present as species of Fe(II). During preparation for analysis, mixing the sample with NaOH caused the formation of very small needle-like crystals of Na, K blue oxichlorwolframites(V) which then easily redissolved into the solution.

Ferberite dissolution took place in solutions saturated with QMM buffer components. Concentration of Al in these solutions was in the range of 0.0003–0.003 mol kg^{-1}, i.e., considerably lower than the W and Fe molality. In the homogeneous, single-phase region of the KCl–HCl system, quartz solubility did not change in experiments with *m*KCl ranging from 0.038 to 2.367. However, quartz solubility decreased reaching 0.022 $m SiO_2$ at 500 °C (Fig. 7.6a) and 0.02 $m SiO_2$ at 400 °C in 8.942 *m*KCl (Fig. 7.6b) experiments. Taking into account such an inadequate character of behavior of SiO_2 and W one can assume that in weakly-acidic concentrated aqueous-salt solutions at 500 °C and NNO buffer a formation of the marked numbers of predominant Si–W heteropolycomplexes did not take place. However, these complexes could be formed when we analyzed quenched solutions for SiO_2 using the blue method (Marczenko 1976) affecting the results to lower $m SiO_2$.

7.4.2 Solid Phases After the Runs

X-ray diffraction and microprobe analysis of the recovered solid phases after the experiments showed that the initial components of the QMM buffer, i.e., Mic, Ms and Qtz, did not undergo phase changes and all three minerals were present in the run products. No new alumina-silicate phases were found, and the compositions of Mic and Ms remained unchanged.

Table 7.1 Experimental results for ferberite $FeWO_4$ solubility in KCl–HCl solutions at QMM buffers

P (MPa)	Time (days)	Initial solution (mol kg^{-1})		Final solution (log *m*)				
		KCl	HCl	W	Fe	Al	SiO_2	HCl^*
1	2	3	4	5	6	7	8	9
500 °C, NNO								
100	18	0.706	0.10	−2.234	−1.970	<−3.5	−1.468	−1.9
100	22	0.706	0.01	−1.941	−2.654	<−3.4	−1.457	−2.1
100	18	2.367	0.10	−1.787	−1.272	<−3.5	−1.414	−1.9
100	22	2.367	0.01	−1.691	−1.487	<−3.4	−1.430	−1.9
100	18	4.471	0.10	−1.680	−0.980	<−3.5	−1.455	−1.9
100	22	4.471	0.01	−1.380	−1.121	<−3.1	−1.493	−2.2
100	18	8.942	0.10	−1.683	−0.812	<−3.5	−1.704	−3.7
100	22	8.942	0.01	−1.260	−1.045	<−3.4	−1.613	−3.6
50	25	0.706	0.10	−2.712	−1.355	−3.0	−1.782	−1.2
50	27	0.706	0.01	−2.800	−1.642	−3.1	−1.835	−1.2
50	25	2.367	0.10	−2.146	−1.022	−2.9	−1.599	−1.0
50	27	2.367	0.01	−1.655	−1.250	−3.2	−1.661	−1.4
50	25	3.353	0.10	−1.995	−0.914	−3.2	−1.557	−1.3
50	27	4.471	0.01	−1.181	−1.073	−3.2	−1.556	−1.7
50	25	4.471	0.10	−1.778	−0.882	−3.0	−1.523	−1.5
50	27	5.749	0.01	−1.173	−1.101	−3.2	−1.512	−2.2
40	40	0.706	0.10	−2.536	−1.224	−2.5	−1.724	−1.0
40	28	0.706	0.01	−2.459	−1.352	−2.5	−1.745	−0.9
40	40	2.367	0.10	−2.152	−0.991	−3.1	−1.852	−1.3
40	28	2.367	0.01	−1.840	−1.147	−3.0	−1.816	−1.4
40	40	4.471	0.10	−1.692	−0.887	−3.2	−1.883	−1.4
40	28	4.471	0.01	−1.419	−1.061	−3.0	−1.914	−1.7
40	40	8.942	0.10	−1.177	−0.888	−3.3	−2.009	−2.4
40	28	8.942	0.01	−0.988	−0.983	−3.3	−1.786	−3.3
500 °C, HM								
100	18	0.706	0.01	−2.911	−2.017	−1.574	n.a.	−1.9
100	22	0.706	0.001	−2.505	−1.934	−1.603	n.a.	−1.9
100	18	2.367	0.01	−2.287	−1.540	−1.688	n.a.	−1.7
100	22	2.367	0.001	−1.965	−1.456	−1.496	n.a.	−1.9
100	18	4.471	0.01	−2.284	−1.437	−1.697	n.a.	−2.7
100	22	4.471	0.001	−1.744	−1.355	−1.692	n.a.	−3.0
100	18	8.942	0.01	−2.202	−1.465	−1.986	n.a.	−3.7

(continued)

Table 7.1 (continued)

P (MPa)	Time (days)	Initial solution (mol kg^{-1})		Final solution (log *m*)				
		KCl	HCl	W	Fe	Al	SiO_2	HCl*
1	2	3	4	5	6	7	8	9
100	22	8.942	0.001	−1.915	−1.383	−2.062	n.a.	−3.9
50	25	0.706	0.01	<−4.1	−1.646	−1.750	n.a.	−1.8
50	27	0.706	0.001	−2.584	−1.792	–	n.a.	−1.5
50	25	2.367	0.01	−2.067	−1.455	−1.688	n.a.	−1.9
50	27	2.367	0.001	−1.882	−1.692	–	n.a.	−1.6
50	25	4.471	0.01	−1.742	−1.306	−1.556	n.a.	−2.7
50	27	4.471	0.001	−1.713	−1.675	–	n.a.	−2.3
50	25	5.749	0.01	−1.564	−1.261	−1.609	n.a.	−3.1
50	27	5.749	0.001	−1.567	−1.645	–	n.a.	−3.0
40	40	0.706	0.01	−2.997	−1.663	−1.971	n.a.	−1.7
40	28	0.706	0.001	<−4.1	−1.731	–	n.a.	−2.2
40	40	2.367	0.01	−1.926	−1.642	–	n.a.	−2.0
40	28	2.367	0.001	−1.750	−1.702	–	n.a.	−2.5
40	40	4.471	0.01	−2.181	−1.495	−1.737	n.a.	−2.2
40	28	4.471	0.001	−2.143	−1.675	–	n.a.	−1.9
40	40	8.942	0.01	−1.892	−1.526	−1.847	n.a.	−2.7
40	28	8.942	0.001	−1.830	−1.752	–	n.a.	−3.7
400 °C, NNO								
100	24	0.706	0.01	−3.604	−3.768	n.a.	−1.605	−3.0
100	36	0.706	0.001	−3.433	<−4.2	n.a.	−1.640	−3.2
100	24	2.367	0.01	−2.551	−2.467	n.a.	−1.546	−3.5
100	36	2.367	0.001	−2.685	−2.230	n.a.	−1.607	−2.8
100	24	4.471	0.01	−1.831	−1.827	n.a.	−1.594	−2.9
100	36	4.471	0.001	−1.997	−1.817	n.a.	−1.713	2.8
100	24	8.942	0.01	−1.366	−1.359	n.a.	−1.704	−2.6
100	36	8.942	0.001	−1.473	−1.306	n.a.	−1.812	−2.5
25	24	0.706	0.01	−3.566	−2.856	n.a.	−1.853	−3.0
25	36	0.706	0.001	<−4.1	−1.743	n.a.	−2.151	−2.0
25	24	2.367	0.01	−2.833	−2.279	n.a.	−1.727	−3.0
25	36	2.367	0.001	−2.300	−1.810	n.a.	−1.845	−2.2
25	24	3.353	0.01	−2.398	−2.104	n.a.	−1.685	−3.0
25	36	3.353	0.001	−2.097	−1.716	n.a.	−1.867	−2.5
25	24	4.471	0.01	−2.000	−1.867	n.a.	−1.682	−3.0

(continued)

Table 7.1 (continued)

P (MPa)	Time (days)	Initial solution (mol kg^{-1})		Final solution (log *m*)				
		KCl	HCl	W	Fe	Al	SiO_2	HCl*
1	2	3	4	5	6	7	8	9
25	36	4.471	0.001	−1.696	−1.589	n.a.	−1.891	−2.6
20	24	0.706	0.01	−3.490	−2.070	n.a.	−2.392	−1.8
20	36	0.706	0.001	−3.577	−1.389	n.a.	−2.061	−1.2
20	36	2.367	0.01	−2.132	−2.132	n.a.	−1.886	−3.8
20	36	2.367	0.001	−2.131	−1.197	n.a.	−2.013	−1.7
20	24	4.471	0.01	−1.629	−1.422	n.a.	−1.827	−1.9
20	24	4.471	0.01	−1.645	−1.447	n.a.	−1.859	−1.7
20	24	8.942	0.01	−1.409	−1.340	n.a.	−1.820	−2.5
20	36	8.942	0.001	−1.234	−1.088	n.a.	−1.973	−2.6

* The molality of HCl was estimated from pH measurement of the quenched diluted solution

Among W-bearing minerals, indent in addition to the initial ferberite, a new phase was found represented by elongated black crystals. SEM analysis indicated the composition corresponded to a chemical composition similar to the K–W bronzes (PTB) K_xWO_3. The small quantities of PTB (<<5 wt%) found did not allow for positive identification using X-ray diffraction. The largest crystals (10–50 μm thick) were chosen for microprobe analysis. The analytical results indicate their composition at 500 °C, 100 MPa corresponded to the formula $K_{0.24\pm0.01}WO_3$ (19 tests, runs in 25 and 40 wt% KCl and 0.1 *m*HCl), at 50 MPa $K_{0.23\pm0.01}WO_3$ (11 tests, run in 25 wt% KCl and 0.1 *m*HCl), and at 40 MPa $K_{0.21\pm0.02}WO_3$ (15 tests, run in 40 wt% KCl and 0.1 *m*HCl). We did not find additional system components present in PTB. A detailed study of ferberite crystals showed however, that in some crystals there occurred an increase in the W/Fe molar ratio during the experiment and an accompanying accumulation of potassium was observed. One can assume that such crystals represented thin growths of ferberite and PTB.

7.5 Thermodynamic Simulations

In solving the problem of the behavior and conditions of ore deposition in hydrothermal deposits, an important role is played by the solubility of ore minerals and the forms of the existence of ore components in their equilibrium solutions. The main component of hydrothermal fluid in tungsten deposits in greisenes is alkali metal chlorides, which concentrations vary widely from 0 to 60 wt% (Wood and Vlassopoulos 1989; Wood and Samson 2000; Gao et al. 2014). In these solutions, according to various researchers, tungsten could exist in the form of tungsten acid $H_2WO_4^0$, the

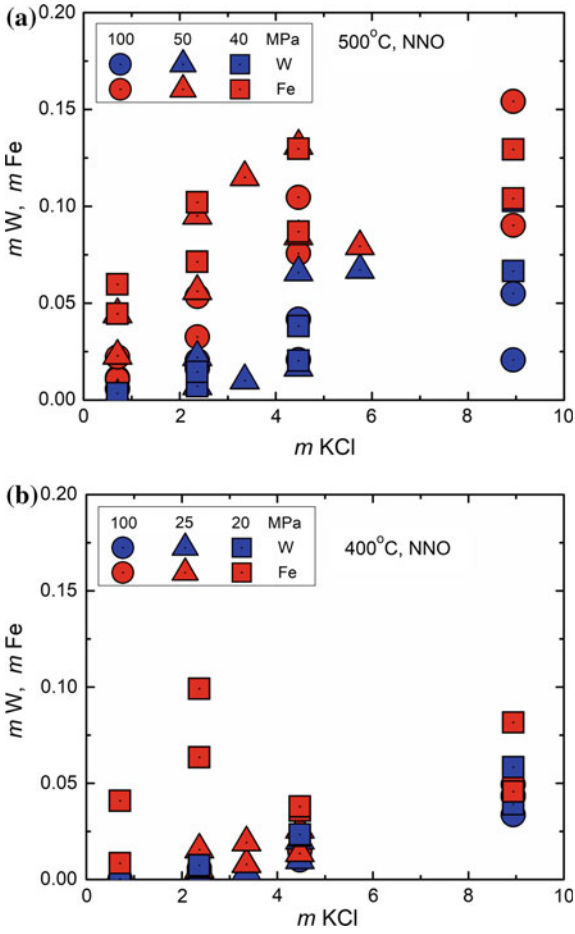

Fig. 7.4 W and Fe concentrations (mol kg^{-1}) in equilibrium with ferberite in the KCl–HCl–H_2O system buffering by QMM and NNO at 500 (**a**) and 400 °C (**b**)

products of its dissociation HWO_4^-, WO_4^{2-} (Ivanova and Khodakovskii 1972) and polymerization $W_4O_{13}^{2-}$ (Bryzgalin 1976), $H_7(WO_4)_6^{5-}$, $H_{10}(WO_4)_6^{2-}$ (Wesolowski et al. 1984), associations with alkaline metal ions $NaHWO_4^0$ (Wood and Vlassopoulos 1989; Wood and Samson 2000), chlorine $WO_2Cl_2^0$ (Veispäls 1979) and mixed form such as HWO_3Cl^0, $NaWO_3Cl^0$ (Khodorevskaya et al. 1990; Kolonin and Shironosova 1991). It is generally not possible to identify species, as the existing experimental data are not sufficient for this purpose. Therefore, the relevance of studies of W complexation in hydrothermal systems in connection with the problem of transport and deposition of tungsten minerals (Eugster 1986; Kolonin and Shironosova 1991; Volina and Barabanov 1995) is still unaddressed.

To describe the solubility of W-containing minerals at high *T*-*P* parameters, there are mutually agreed thermodynamic data (equilibrium constants and Gibbs free energies) for only 5 species W(VI): $H_2WO_4^0$, HWO_4^-, WO_4^{2-}, $NaHWO_4^0$ and $NaWO_4^-$ (Wood and Samson 2000). For the species $KHWO_4^0$ and KWO_4^- approximation of

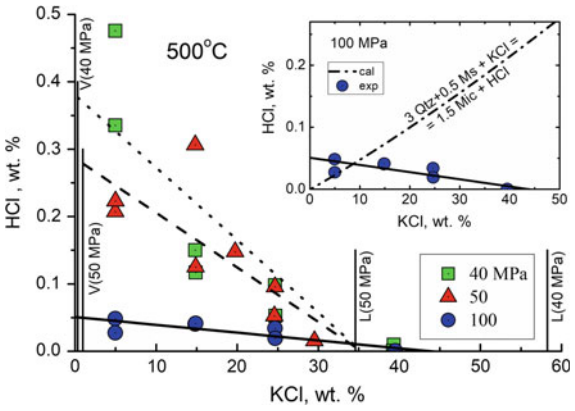

Fig. 7.5 Total quench HCl results as a function of KCl concentration in the experiments on ferberite solubility in Qtz-Mic-Ms-Ni-NiO buffered system at 500 °C and 40, 50, 100 MPa and their correlation with calculated values of HCl and KCl of the alumina-silicate buffer assemblage at 100 MPa. The dotted, dashed and solid lines are results of linear fit in addition to the L, V lines

the association constants has been evaluated. The data on particles and complexes of W(V) are completely absent, although in experiments on the solubility of WO_3 and (Fe, Mn)WO_4 in NaCl solutions, the formation of tungsten blue with a variable content of W(VI)/W(V) occurred (Bryzgalin 1976; Wesolowski et al. 1984; Manning and Henderson 1984; Wood and Vlassopoulos 1989; Zaraisky 1995; Redkin et al. 1999). These compounds, according to the composition and X-ray data, corresponded to sodium tungsten bronzes, Na_xWO_3, where x = 0.1–0.4, and were formed already at fO_2 with the oxygen buffer corresponding to Fe_2O_3–Fe_3O_4 (Red'kin 2000). The effect of fO_2 on the solubility of wolframite and its extreme members of ferberite and hubnerite (huebnerite) ($MnWO_4$) has not been considered.

We used numerical simulation of the Qtz + Mic + Ms + Ferb with KCl–HCl–H_2O solution at 400–500 °C and 100 MPa in an open system with fO_2 corresponding to the Ni–NiO (NNO: $fO_2 = 10^{-22.423}$ Pa at 400 °C–$10^{-17.706}$ Pa at 500 °C) and Fe_2O_3–Fe_3O_4 (HM: $10^{-13.63}$ Pa at 500 °C) buffers to determine the composition of the W complexes (Robie and Hemingway 1995). Determination and refinement of thermodynamic properties of aqueous solution species is solved using the software package HCh (Shvarov and Bastrakov 1999) and the program supporting technology OLE Automation (Shvarov 2008), realized in the program OptimA (Shvarov 2015). Thermodynamic properties of most simple particles and complexes K^+, KCl^0, KOH^0, Na^+, $NaCl^0$, $NaOH^0$, SiO_2aq^0, $HSiO_3^-$, Fe^{2+}, WO_4^{2-}, Cl^-, H_2O, OH^-, H^+, were taken from SUPCRT'92 (Johnson et al. 1992; Shock et al. 1997), aluminum species Al^{3+}, $AlOH^{2+}$, $Al(OH)_2^+$, $HAlO_2^0$ $Al(OH)_3^0$, AlO_2^- $Al(OH)_4^-$ by Pokrovskii and Helgeson (1995), Gibbs Free energy of HCl^0, by Hemley et al. (1992), $FeCl^+$, $FeCl_2^0$ by Wood and Samson (2000). Free energy and HKF parameters of hydroxo and chloride complexes Fe(II): $Fe(OH)^-$, $FeOaq^0$, $HFeO_2^-$, $FeCl^+$ and $FeCl_2^0$ are calculated from the equilibrium constants of the hydrolysis reactions presented in Wood and Samson

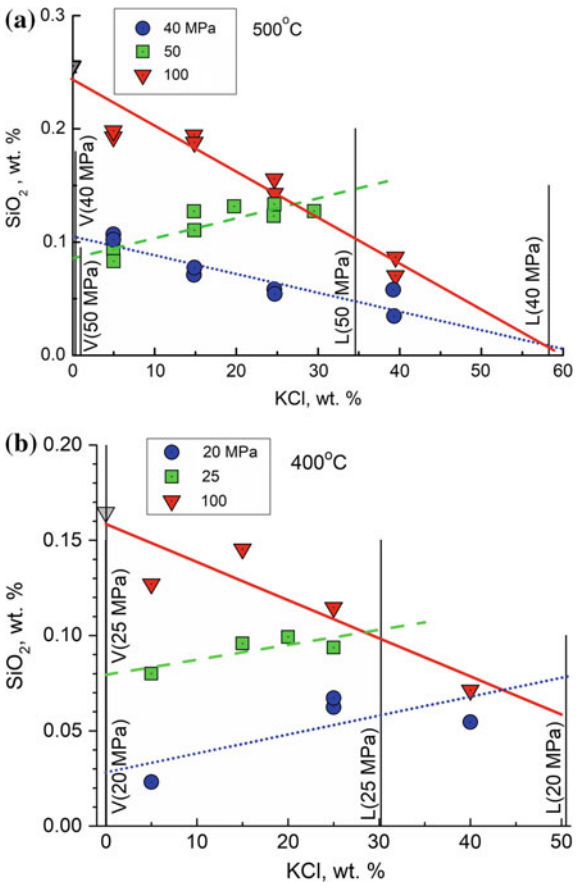

Fig. 7.6 The dependence of dissolved silica (in wt%) from Qtz-Mic-Ms buffers on the initial KCl concentration in experiments at 500 (**a**) and 400 °C (**b**), their approximation by linear fit (solid and dashed lines) and calculated quartz solubility in relation to Si species composition at 1000 bar. Vertical lines show KCl concentration in vapor 'V' and liquid 'L' phases at the corresponding pressure in MPa

(2000). For Fe(III): $FeOH^{2+}$, $Fe(OH)_2^+$, $Fe(OH)_3^0$, $Fe(OH)_4^+$ hydroxocomplexes the best convergence of the calculated and data free energies was obtained using the approximation of the stability constants of the complexes (Wood and Samson 2000) modified Ryzhenko-Bryzgalin equation (Ryzhenko 1981; Bryzgalin and Ryzhenko 1981; Bryzgalin and Rafalsky 1982). The contribution of Fe(III) species to the total iron concentration was negligible (Wood and Samson 2000).

We did not consider the species of the $KFeCl_3^0$ composition, although according to Tagirov (1998), the contribution of these particles to the total solubility of the iron-containing phases in highly concentrated water-salt solutions may be dominant.

The activity coefficients of aqueous species with were calculated using an extended Debye-Hückel equation

$$\log \gamma_i = -\frac{Az_i^2\sqrt{I}}{1 + B\mathring{a}\sqrt{I}}, \tag{7.5}$$

where I (mol kg^{-1}) stands for ionic strength of the solution, A and B represent the Debye Hückel coefficients for pure solvent dependent on P, T; z_i is the charge and $\mathring{a}$ is the ion size parameter that was accepted after Rafalsky (1973) to be equal 4.5 Å for all species.

The free energies of formation of quartz (Qtz) and microcline (Mic) are taken as the basis for solid mineral phases (Robie et al. 1978). The free energies of Ab (albite), And (andalusite), Ms, Prg (paragonite), Pf (pyrophillite) were corrected according to experimental constants of hydrolysis reactions (Hemley and Jones 1964) and taken as stable phases in the system K_2O–Na_2O–Al_2O_3–SiO_2–H_2O–HCl at 500–400 °C and 100 MPa.

For reaction (7.1), which served in our experiments as an acid-base buffer, the accepted value for the equilibrium ratio log mKCl/mHCl = 2.08 (at 500 °C, 100 MPa) and 2.70 (at 400 °C, 100 MPa) (Hemley 1959; Redkin 1983). This also led to an aluminum saturation concentration corresponding to our experimental data (approximately 10^{-4}–10^{-5} mol kg^{-1} H_2O).

When calculating the free energies of ferberite, we used the equilibrium constants of the reaction of dissolving ferberite calculated at 400 and 500 °C and 100 MPa according to Wood and Samson (2000):

$$FeWO_{4(s)} + 2HCl^0 = H_2WO_4^0 + FeCl_2^0, \tag{7.6}$$

pK(6) = 3.2 and 3.0, respectively.

When determining the composition of aqueous species and the valence state of tungsten in solutions (see Table 7.1) with the parameters of the experiments, the following assumptions were taken into account;

1. Most aqueous tungsten was assumed to be present as complex of W(V) as the cooled solutions were W, colorless and transparent despite high concentrations (mW$_{total}$ > 0.002 mol kg^{-1}). When performing chemical analyzes on tungsten, using the colorimetric method with bromopyrogallol red in the presence of cetylpyridinium bromide as a surfactant (Mamedova et al. 2004), it was noted that the solutions after the experiments when mixed with a strong alkali, with the addition of hydroxylamine, actively interacted, producing small ammonia bubbles (alkaline reaction of the wet indicator paper in the atmosphere of bubbles). These gas bubbles dissolved in the liquid phase. It is known (Brikun et al. 1967) that strong reducing agents (HI, H_2S, $SnCl_2$, zinc dust, etc.) reduce hydroxylamine to NH_3. Since there were no other reducing agents in the solutions, it is reasonable to assume that the species W(V) or even W(IV) behaved as the reducing agent in the analyzed solutions.

An additional but indirect argument for the presence of W(V) can be potassium tungsten bronzes K_xWO_3 (PTB), where x = 0.20–0.24, which is formed in the experiments and represents compounds of W(V, VI).

2. W(V) in solution at high temperature is represented by monomeric and polymeric species, which may include K^+, Cl^-, OH^-, H_2O. Silica-12-tungsten acid and its salts $K_{4-x}H_x[SiW_{12}O_{40}] \cdot nH_2O$ (x = 0–4, n = 5, 14, 24 or 30), as well as other silica heteropolytungstate compounds were not formed in appreciable amounts. This follows from the analysis of solubility data of quartz (Table 7.1 and Fig. 7.6a, b) at 500 and 400 °C and 100 MPa.
3. Changes in the acidity of the solutions may be mainly due to hydrolysis or dissociation of tungsten compounds upon cooling, since ferrous chloride species, $FeCl^+$ and $FeCl_2^0$, which are stable in the test mode, do not hydrolyze when cooled to room temperature, but completely dissociate into Fe^{2+} and Cl^- without changing $m\mathrm{HCl}_{\mathrm{total}}$ ($m\mathrm{HCl}^0 + m\mathrm{H}^+$).

For test the calculated and experimental data of congruent and incongruent (with the formation of PTB-02, $K_{0.2}WO_3$) solubility of ferberite, presented in Table 7.1, we examined more than 15 W(V) species containing from 1 to 6 tungsten atoms and having a charge of +1 to −3, as well as 5 anionic species with a charge of − 1 to −3, containing both W(V) and 20–66 mol% W(VI). The $KHWO_4^0$ and KWO_4^- species proposed in Wood and Samson (2000), line WS in Figs. 7.7 and 7.8 were the dominant contributors to the solubility of ferberite in strong KCl solutions, but did not reflect the effect of fO_2, were omitted from consideration.

We assumed that W(V) compounds as well as compounds W(VI) compounds in a hydrothermal solution will have similar structure. This was taken into consideration when selecting the composition of possible aqueous species W(V).

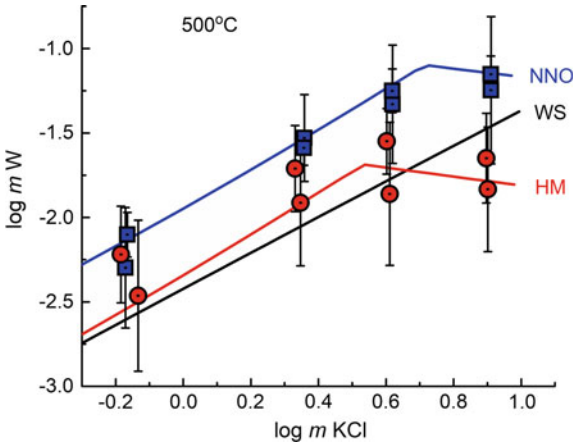

Fig. 7.7 Influence of mKCl on mW in a solution equilibrated with ferberite in the QMM buffered system at 500 °C and 100 MPa by experimental (symbols) and calculated (lines) data. The WS line is from calculations by Wood and Samson (2000)

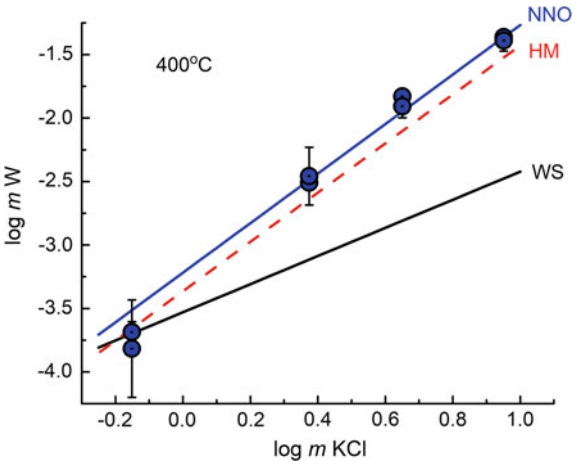

Fig. 7.8 Influence of *m*KCl on *m*W in a solution equilibrated with ferberite in the QMM buffered system at 400 °C and 100 MPa by experimental (symbols) and calculated (lines) data. The WS line is from calculations by Wood and Samson (2000)

According to the data presented in Table 7.1, the total concentrations of iron and tungsten in the solutions after the experiment were differed. This could be due to the initial purity of synthetic ferberite (a slight excess of iron oxide), an insufficient amount of quartz, and the formation of a containing phase in the course of the experiment, i.e. potassium tungsten bronzes (PTB). The congruent solubility of ferberite in potassium chloride solution, with an acidity given by Qtz-Mic-Ms buffer, can be calculated by the equation

$$m\mathrm{FeWO_4} = \sqrt[\alpha+1]{(m\mathrm{W_{total}})^{\alpha} \times m\mathrm{Fe_{total}}}, \tag{7.7}$$

where $\alpha = \sum_i \frac{\alpha_i}{i}$, $\alpha_i = \frac{i \cdot m\mathrm{W}_i}{m\mathrm{W_{total}}}$ mol fractions of fluid species containing the same number i of atoms W, taking into account the fractions of species of different degrees of polymerization in calculations using the obtained equilibrium constants. Considering that the main contribution to $\mathrm{W_{total}}$ is made by W(V, VI) species in the form of monomers, Eq. (7.7) can be simplified to the form

$$m\mathrm{FeWO_4} = \sqrt{(m\mathrm{W_{total}} \times m\mathrm{Fe_{total}})}, \tag{7.8}$$

representing the geometric mean of the concentrations of tungsten and iron. In Fig. 7.7, square and round symbols show the solubility of ferberite calculated using Eq. (7.8) for NNO and HM buffers, respectively. Extreme concentrations of $\mathrm{W_{total}}$ and $\mathrm{Fe_{total}}$ are accepted for the magnitude of the $m\mathrm{FeWO_4}$ definition error.

The best agreement of experimental and calculated data (see Fig. 7.7) at 500 °C and 100 MPa was achieved for two newly introduced species $\mathrm{WO_3^-}$ (or $\mathrm{H_2W^VO_4^-}$)

and $H_2W_2O_7^-$ ($H_2W^VW^{VI}O_4^-$). According to calculations, $FeCl_2^0$ are the predominant iron species in solution at both NNO and HM oxygen buffers over the entire KCl concentration range studied. The structure of the predominant tungsten species, conversely, depended on both fO_2, and mKCl. At HM buffer conditions the W(VI) content ranged from 32 to 43.5% of mW_{total} in the mKCl range from 0.3 to 7.7. At low concentrations of KCl, tungsten-bearing species WO_3^-, HWO_4^-, $H_2W_2O_7^-$ (in order of importance) prevailed, while in concentrated solutions the $H_2W_2O_7^-$ species dominated.

At NNO buffer conditions, calculations indicate the WO_3^- and $H_2W_2O_7^-$ species dominated in the mKCl range investigated. W(VI) concentrations increased in solution from 9 to 34.8% with increasing mKCl from 0.3 to 5.3. Incongruent dissolution of Ferb with concurrent formation of PTB and a slight decrease in both mW_{total} and fraction of W(VI) in solution (Fig. 7.7) shows good agreement between calculated and experimental data.

The influence of potassium chloride concentration on solubility of the ferberite in the solutions at 400 °C, 100 MPa, NNO buffer and at the acidity given by Mic-Ms-Qtz buffer is shown in Fig. 7.8. The slope of mW with mK at 400 °C is steeper than at 500 °C. This indicates that there are aqueous tungsten species present that contain more than 2 W atoms. The best agreement between the experimental and calculated data (see Fig. 7.8) was obtained by introducing the species $W_5O_{16}^{3-}$ (or $W^VW_4^{VI}O_{16}^{3-}$) previously proposed in the work (Redkin and Kostromin 2010). According to calculations, the fraction of the $W_5O_{16}^{3-}$ species increases dramatically at mKCl > 0.05 reaching 99% in the solution containing 0.7 mKCl. At the same time, the share of W(V) is 20% of the particles concentration of $W_5O_{16}^{3-}$. In Fig. 7.8 (WS line) also shows the results of calculations based on data (Wood and Samson 2000) using $KHWO_4^0$ and KWO_4^- species.

Concentrations of sodium salts in natural hydrothermal solutions are typically greater than that of potassium, therefore we made calculations for ferberite solubility in solutions of NaCl–KCl–HCl. Since the composition of ore-bearing solutions can only be assumed, but since it is known the hydrothermal solutions produce quartz-muscovite alteration in the host rocks, it is possible to speculate on geochemical boundary conditions. The Qtz + Ms association field at 500 and 400 °C, 100 MPa and constant mCl is limited by the following non-variant points: Qtz-Ab-Mic-Ms (1), Qtz-Ab-Prg-Ms (2) and Qtz-And-Prg-Ms (3 at 500 °C) or Qtz-Pf-Prg-Ms (3 at 400 °C) after Hemley and Jones (1964). If the concentration of chlorides in a system changes, then non-variant points turn into the hydrolysis equilibria, which determine the mKCl/mHCl and mNaCl/mHCl ratios. Thus, the solubility of ferberite on the lines of hydrolysis reactions of aluminosilicates will correspond to extreme values. The systems in which iron oxides are present are also of interest. Calculations show that at low chloride concentrations, magnetite accompanies ferberite.

Figures 7.9 and 7.10 show the results of the calculations at 400 and 500 °C and pressure of 100 MPa. As expected, the solubility of Ferb increases with the increasing temperature, mCl (mNaCl + mKCl), $f(H_2)$, mKCl/mHCl (or when changing associations 1 → 3) and decreases in the presence of Mgt. The maximum solubility of ferberite is found in KCl solutions equilibrated with Qtz-And-Ms at 500 °C or

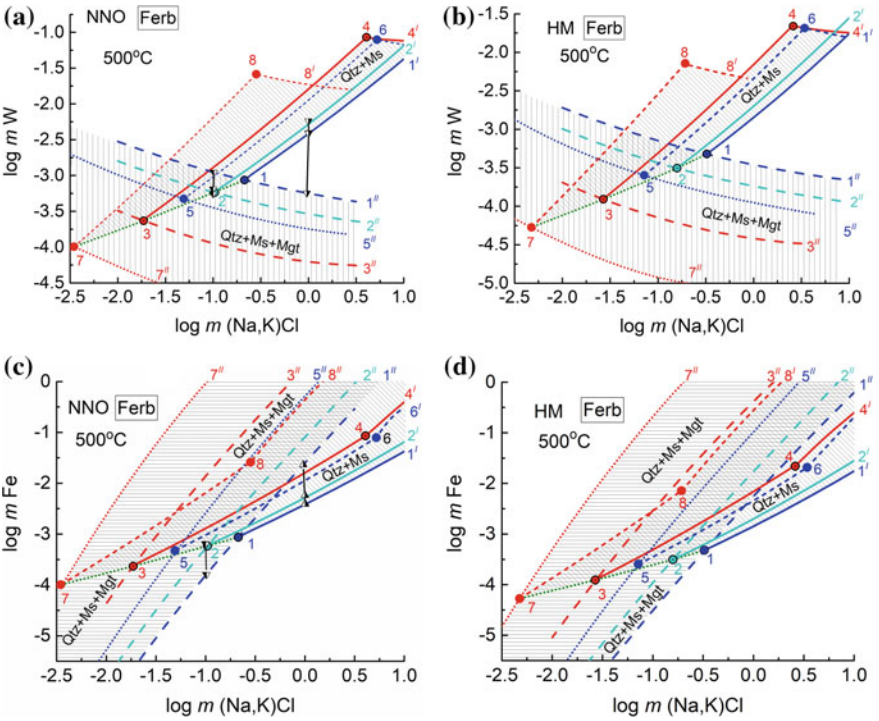

Fig. 7.9 The projections of 3D surfaces of ferberite solubility on the *m*(Na, K)Cl–*m*W and *m*(Na, K)Cl–*m*Fe plane at 500 °C, 100 MPa, NNO (**a**, **c**) and HM (**b**, **d**) buffers in chloride solutions controlled by various alumina-silicate assemblages. *Legend* 1—nonvariant point (NP) Qtz + Ab + Mic + Ms + Ferb + Mgt; 2—Qtz + Ab + Prg + Ms + Ferb + Mgt; 3—Qtz + And + Ms + Prg + Ferb + Mgt; 4—Qtz + And + Ms + Prg + Ferb + PTB-02; 5—Qtz + Mic + Ms + Ferb + Mgt (NaCl free solutions); 6—Qtz + Mic + Ms + Ferb + PTB-02 (no NaCl); 7—Qtz + And + Ms + Ferb + Mgt (no NaCl); 8—Qtz + And + Ms + Ferb + PTB-02 (no NaCl); 1′, 2′, 4, 6—lines of saturation of solutions with Ferb (congruent dissolution); 4′ and 6′—Ferb + PTB, 1″, 2″, 3″, 4″, 5″, 7″, 8″—Ferb + Mgt, correspondingly; the shaded areas show the limits of variation in the concentrations of tungsten (**a**, **c**) and iron (**b**, **d**) for the Qtz + Ms + Ferb and Qtz + Ms + Ferb + Mgt, respectively

Qtz-Pf-Ms at 400 °C. Further change in the composition of solution towards reduction of *m*KCl/*m*HCl will cause the formation of andalusite (or pyrophyllite), and in solutions containing fluorine—topaz. Therefore, solutions saturated with ferberite, marked by hatching in these figures, are of practical interest for modeling tungsten ore formation. From the data obtained, it follows that at 500 °C the change in $f(O_2)$ from NNO to HM buffer reduces the tungsten concentrations in solution by 1.5–2.7 times, and at 400 °C by 1.4 times.

The influence of aluminosilicate assemblage and the presence of magnetite on the content of tungsten and iron in solution saturated with ferrite is of interest. Figure 7.9a, c and 7.10a, b triangular symbols show trends of the changing *m*W and *m*Fe in solution initially equilibrated with the Qtz-Ms-Ferb assemblage, then interacting with wall

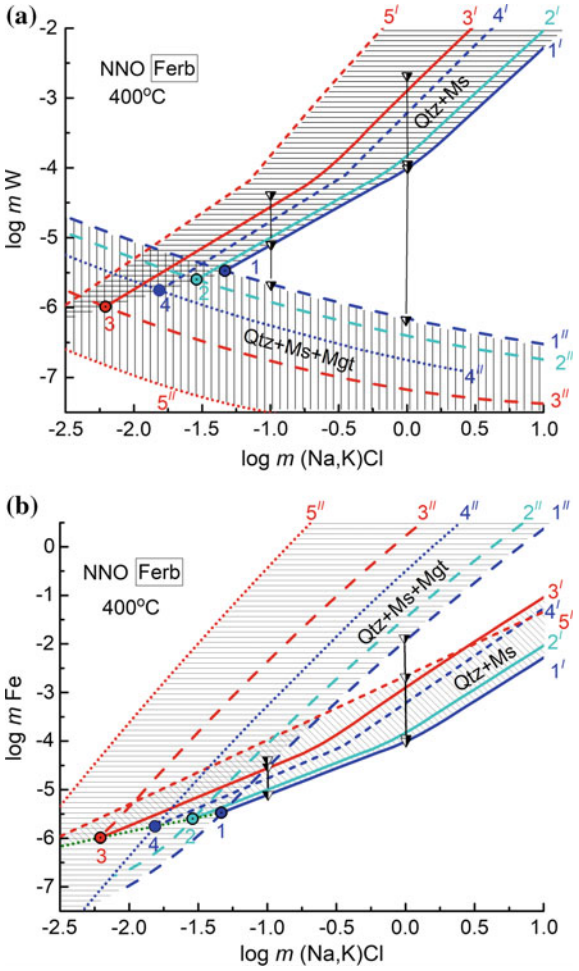

Fig. 7.10 The projections of 3D surfaces of ferberite solubility on the *m*(Na, K)Cl–*m*W (**a**) and *m*(Na, K)Cl–*m*Fe (**b**) plane at 400 °C, 100 MPa, NNO buffer in chloride solutions controlled by various alumina-silicate assemblages. *Legend* 1—nonvariant point Qtz + Ab + Mic + Ms + Ferb + Mgt; 2—ND Qtz + Ab + Prg + Ms + Ferb + Mgt; 3—Qtz + Pf + Ms + Prg + Ferb + Mgt; 4—Qtz + Mic + Ms + Ferb + Mgt (no NaCl added); 5—Qtz + Pf + Ms + Ferb + Mgt (no NaCl); 6—Qtz + Mic + Ms + Ferb + PTB-02 (no NaCl); 1′, 2′, 3′, 4′, 5′—congruent dissolution of Ferb; 1″, 2″, 3″, 4″, 5″,—Ferb + Mgt; the shaded areas show the limits of variation in the concentrations of tungsten (**a**) and iron (**b**) for the Qtz + Ms + Ferb and Qtz + Ms + Ferb + Mgt, respectively

rocks containing Mic, Ab, Mgt. In solutions containing 0.76 *m*NaCl + 0.24 *m*KCl + 0.01 *m*HCl, equilibrated at 500 °C with Qtz-Ms-Ferb assemblage, the smallest change (1.4 times) is due to the appearance of Mic and Ab, while saturation of the solution with magnetite reduces the initial *m*W by 10 times. In 0.1 *m*Cl solution of 0.076 *m*NaCl + 0.024 *m*KCl + 0.001 *m*HCl, the *m*W variations are less obvious

and have the opposite tendency, i.e. the appearance of magnetite in association with Qtz-Ms-Ferb leads to a slight decrease in *m*W, while saturation of the solution with albite, microcline and magnetite from side rocks increases the solubility of ferberite (*m*W) (see Fig. 7.9a).

The solution containing 0.76 *m*NaCl + 0.24 *m*KCl + 0.01 *m*HCl, equilibrated at 400 °C and 100 MPa with Qtz-Ms-Ferb assemblage, contains 0.002 *m*W. The interaction of such a solution with side rocks containing Mic or Mic + Ab, leads to the deposition of 94.5–95.2% tungsten in the form of ferberite from the solution, while the presence of Mgt in wall rocks reduces the concentration of tungsten in the affecting solution by 99.97% (Fig. 7.10). Tungsten content in the 0.076 *m*NaCl + 0.024 *m*KCl + 0.001 *m*HCl equilibrium solution with the Qtz-Pf-Ms-Ferb assemblage is 50 times lower, than in the 1.0 *m*Cl solution. Although tungsten deposition from this solution due to geochemical barriers associated with the appearance of Mic and Mgt in the host or wall rocks is very significant (from 80 to 95%), solutions containing 0.1 *m*Cl cannot be considered promising for the formation large deposits of tungsten ores associated with granites.

Particular attention should be paid to the effect of temperature and wall rock mineralogy on the solubility of ferberite. Figure 7.11 shows a case when the chloride solutions containing 1.0 and 0.1 *m*Cl are first equilibrated at 500 °C and 100 MPa with Qtz-Ms-Ferb assemblage are than isobarically cooled to 400 °C, imposing the solutions to interact with wall rocks containing feldspars and magnetite. Calculations indicate that the decrease in temperature of hydrothermal ore-bearing solution and its interaction with both feldspars and magnetite leads to the deposition of 99% of

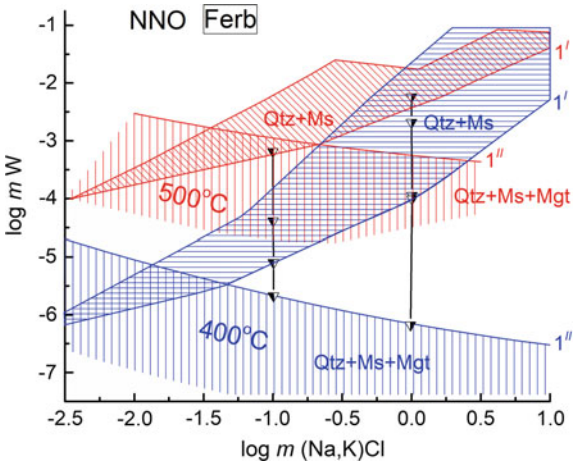

Fig. 7.11 Influence of temperature, *m*KCl and wall rock minerals (Mic, Ab, Mgt) on *m*W change in solutions initially equilibrated with the quartz-muscovite-ferberite assemblage at 500 °C, 100 MPa, NNO (the projections of 3D surfaces of ferberite solubility on the *m*(Na, K)Cl–*m*W plane). *Legend* 1′—nonvariant equilibria Qtz + Ab + Mic + Ms + Ferb; 1″—Qtz + Ab + Mic + Ms + Ferb + Mgt

tungsten. Moreover, taking into account the high solubility of ferberite at 500 °C and 100 MPa in 0.1 *m*Cl solution (6.5×10^{-4} *m*W), such solutions can be considered as ore-bearing ones.

The presented results of thermodynamic modeling were performed for a homogeneous region of NaCl–KCl–HCl–H_2O fluid. In the region of immiscibility, the water-salt fluid splits into two equilibrium fluids of different densities, containing different amounts of HCl and (Na, K)Cl, which have a major influence on the peculiarity of dissolving ferberite in coexisting fluid phases.

The thermodynamic calculations used for a homogeneous solution cannot be used for the region of the fluid immiscibility (Redkin et al. 2015). As soon as apparent solubility of ferberite on concentration of KCl in two-phase region corresponds to Eq. (7.4) we can calculate the solubility of ferberite in the V- and L-phases of KCl fluid. The results of calculations in wt% are shown in Table 7.2. The correlations between apparent solubility of ferberite and concentration of KCl in the two-phase region are given in the right-hand column. The values of S_{FeWO4} obtained clearly demonstrate its dependence on fO_2. Otherwise the ferberite dissolution has to be considered as a redox reaction in range fO_2 from $10^{-17.7}$ (NNO) to $10^{-13.63}$ Pa (HM) at 500 °C. Taking in account that the predominant valence of iron relates to Fe(II) as in ferberite as well as in solute species, because high dissolution of iron in the system studied, W can change valance only from W(VI) in ferberite to W(V or IV) in solution.

Table 7.2 Estimated values of ferberite solubility in vapor and liquid phases of the fluid KCl–HCl–H_2O

T (°C)	P (MPa)	V-phase (wt%)		L-phase (wt%)		fO_2	Correlations used
		KCl	$FeWO_4$	KCl	$FeWO_4$	Buffer	Ferberite solubility (S) (wt%)
500	50	0.96	0.21	34.59	2.03	NNO	$S = 0.154 + 0.0543 \cdot C_{KCl}$ ($\pm$ 0.15)
500	40	0.32	0.50	58.25	2.57	NNO	$S = 0.493 + 0.0356 \cdot C_{KCl}$ ($\pm$ 0.11)
500	50	0.96	0.19	34.59	0.77	HM	$S = 0.178 + 0.017 \cdot C_{KCl}$ ($\pm$ 0.15)
500	40	0.32	0.34	58.25	0.36	HM	$S = 0.342 + 0.00032 \cdot C_{KCl}$ ($\pm$ 0.15)
400	25	0.067	0.001	30.00	0.41	NNO	$S = 5 \cdot 10^{-5} + 0.0136 \cdot C_{KCl}$ ($\pm$ 0.15)
400	20	0.011	0.1	51.16	1.33	NNO	$S = 0.101 + 0.024 \cdot C_{KCl}$ ($\pm$ 0.15)

7.6 Conclusions

1. Ferberite dissolution in KCl solutions under pH and fO_2 buffered conditions (Qtz-Mic-Ms, and NNO or HM) at 400–500 °C behaves both congruently as well as incongruently with accompanying potassium tungsten bronzes formation (PTB), K_xWO_3, (x = 0.2–0.3).
2. Using bulk composition data, the congruent and apparent solubility of ferberite at 400 and 500 °C in homogeneous KCl–HCl solutions at $P = 100$ MPa and in the region of fluids immiscibility at $P = 20$, 25, 40, and 50 MPa has been estimated. Tungsten concentration values do not show strong pressure dependence, however, there is some solubility increase accompanying pressure decreases in mKCl < 3 mol kg^{-1} solutions.
3. The data at $P = 100$ MPa and mKCl from 0.7 to 3 mol kg^{-1} suggest the general contribution of total tungsten solubility may favor the mononuclear species which, in turn, causes increased acidity of the quenched solution in the homogeneous region. Conversely, in 4.0–8.9 mKCl solutions and in the region of fluids immiscibility at 500 °C, pressure of 40, 50 MPa and $fO_2 = 10^{-17.7}$ Pa (NNO), we identified polynuclear tungsten(V, VI) species contributing to increased alkalinity during quench.
4. As has been shown in thermodynamic calculations at $P = 100$ MPa, the predominant aqueous species of tungsten in KCl–HCl solutions at $fO_2 = fO_2$(NNO) may be W(V, VI) species: WO_3^-, HWO_4^-, $H_2W_2O_7^-$ at 500 °C and HWO_4^-, $W_5O_{16}^{3-}$ at 400 °C.
5. The total mW in equilibrium with ferberite in the aluminosilicate buffered systems depends upon mCl, T and fO_2. Deposition of tungsten from ore-bearing solutions is due to interaction with wall rocks containing feldspars, and iron oxides and decrease of temperature. In the magnetite bearing system, the equilibrium tungsten concentration does not exceed $2 \cdot 10^{-5}$ mol kg^{-1} at 400 °C. Therefore, aqueous tungsten mobility should decrease sharply in iron-enriched rocks.

Acknowledgements This study was suggested through discussions with Dr. J. J. Hemley (USGS), Prof. G. P. Zaraisky (IEM RAS), and Corresponding Member of the RAS V. I. Velichkin (IGEM RAS) about the major role of immiscibility in water-salt systems and its impact on the processes responsible for formation of giant ore deposit systems. The authors are grateful also to T. K. Chevichelova, G. V. Bondarenko, A. N. Nekrasov, O. A. Mozgovaya all from IEM RAS, G. E. Kalenchuk from IGEM RAS, Olga Smetanina for analytical assistance and for their help in manuscript preparation, Prof. A. F. Koster van Groos and David M. Petrovski (USEPA) and the anonymous referees for critical comments on an earlier draft of this paper. Some recalculations and revisions of this manuscript were done after discussion with Prof. S. A. Wood. This research was supported from the Grants of Russian Foundation for the Basic Research and project No AAAA-A18-118020590151-3 of the IEM RAS.

References

Andreeva IYu, Lebedeva LI, Kavelina GL (1992) Determination of small amounts of molybdenum and tungsten as complexes of the metals with bromopyrogallol red and some superactants. Russ J Anal Chem 12:2202–2206 (in Russian)

Basargin NN, Bikova VS, Polupanova LI (1976) Photometric analyses of aluminum in the silicate rocks with the aid of antrazochrom. In: Theoretical and practical questions of organic reagents utilization in the analyses of the mineral objects. Nedra Press, Moscow, pp 119–124 (in Russian)

Brikun IK, Kozlovsky MT, Nikitina LV (1967) Hydrazine and hydroxylamine and their application in analytical chemistry. Nauka, Alma-Ata, 175 p (in Russian)

Bryzgalin OV (1976) On the solubility of tungstic acid in an aqueous salt solution at high temperatures. Geochem Int 13(3):155–159

Bryzgalin OV, Rafalsky RP (1982) Approximate estimation of constants of instability of complexes of ore elements under high temperatures. Geokhimia 6:839–849 (in Russian)

Bryzgalin OV, Ryzhenko BN (1981) Prediction of temperature and baric dependence of the dissociation constants of electrolytes based on the elementary electrostatic model. Geokhimia 12:1886–1890 (in Russian)

Busev AI, Ivanov VM, Sokolova TM (1976) Analytical chemistry of tungsten. Nauka Press, Moscow, 240 p (in Russian)

Cygan GL, Hemley JJ, Doughten MW (1994) Fe, Pb, Zn, Cu, Au, and HCl partitioning between vapor and brine in hydrothermal fluids—implications for porphyry copper deposits. In: USGS research on mineral deposits. Part A, 9th V.E. McKelvey forum, USGS circular 1103-A, pp 26–27

Dadze TP, Sorokin VI, Nekrasov IYa (1981) Solubility of SnO_2 in water and in aqueous solutions of HCl, HCl + KCl, and HNO_3 at 200–400°C and 1013 bar. Geochem Int 18(5):142–152

Eugster HP (1986) Minerals in hot water. Am Mineral 71:655–673

Gao YW, Li Z, Wang J, Hattori K, Zhang Z, Jianzhen GJ (2014) Geology, geochemistry and genesis of tungsten-tin deposits in the Baiganhu District in the Northern Kunlun Belt, Northwestern China. Econ Geol 109:1787–1799

Hemley JJ (1959) Some mineralogical equilibria in the system K_2O–Al_2O_3–SiO_2–H_2O. Am J Sci 257:241–270

Hemley JJ, Jones WR (1964) Chemical aspects of hydrothermal alteration with emphasis on hydrogen metasomatism. Econ Geol 59(4):538–569

Hemley JJ, Cygan GL, d'Angelo WM (1986) Effect of pressure on ore mineral solubilities under hydrothermal conditions. Geology 14:377–379

Hemley JJ, Cygan GL, Fein JB, Robinson GR, d'Angelo WM (1992) Hydrothermal ore-forming processes in the light of studies in rock-buffered system. 1. Iron-copper-zinc-lead sulfide solubility relations. Econ Geol 87:1–22

Hovey JK, Pitzer KS, Tanger JC IV, Bischoff JL, Rosenbauer RJ (1990) Vapor-liquid phase equilibria of potassium chloride-water mixtures: equation-of-state representation for KCl–H_2O and NaCl–H_2O. J Phys Chem 94:1175–1179

Ivanov IP, Chernysheva GN, Dmitrenko LT, Korzhinskaya VS (1994) New hydrothermal facilities to study mineral equilibria and mineral solubilities. In: Experimental problems of geology. Nauka Press, Moscow, pp 706–720 (in Russian)

Ivanova GF, Khodakovskii IL (1972) About the state of tungsten in hydrothermal solutions. Geokhimia 11:1426–1433 (in Russian)

Ivanova GF, Naumov VB, Kopneva LA (1986) Physic-chemical parameters of formation of scheelite in the deposits of various genetic types. Geokhimia 10:1431–1442 (in Russian)

Johnson JW, Oelkers EH, Helgeson HC (1992) SUPCRT92: a software package for calculating the standard molal thermodynamic properties of minerals, gases, aqueous species, and reactions from 1 to 5000 bar and 0° to 1000°C. Comput Geosci 18(7):899–947

Khodorevskaya LI, Tikhomirova VI, Postnova LE (1990) Study of WO_3 solubility in HCl solutions at 450°C. Dokl Akad Nauk SSSR 113(3):720–722 (in Russian)

Klevtsov PV, Novgorodtseva NA, Kharchenko LYu (1970) Hydrothermal synthesis of the $FeWO_4$ crystals. Crystallographia 15(3):609–610 (in Russian)

Kolonin GR, Shironosova GP (1991) The state of the art in the field of experimental studies on tungsten forms in hydrothermal solutions. In: 12th all-union meeting on experimental mineralogy, Miass, USSR, 24–26 Sept 1991, Abstracts, p 58

Kovalenko NI, Ryzenko BN, Barsukov VL (1986) The solubility of cassiterite in HCl and HCl + NaCl (KCl) solutions at 500°C and 1000 atm under fixed redox conditions. Geochem Int 23(7):1–16

Malinin SD, Kurovskaya NA (1996) The effect of pressure on mineral solubility in aqueous chloride solutions under supercritical conditions. Geokhim Int 1(1):45–52

Mamedova AM, Ivanov VM, Akhmedov SA (2004) Interaction of tungsten(VI) and vanadium(V) with pyrogallol red and bromopyrogallol red in the presence of surfactants. Vestn Mosk Univ Ser Chem 45(2):117–123 (in Russian)

Manning DAC, Henderson P (1984) The behaviour of tungsten in granitic melt-vapour systems. Contrib Mineral Petrol 86(3):286–293

Marczenko Z (1976) Spectrophotometric determination of elements. Wiley, New York, 355 p

PDF (1980) Powder diffraction file 1980. Joint Committee on Powder Diffraction Standards, International Centre for Diffraction Data, Swarthmore, PA, USA

Pokrovskii VA, Helgeson HC (1995) Thermodynamic properties of aqueous species and the solubilities of minerals at high pressures and temperatures; the system Al_2O_3–H_2O–NaCl. Am J Sci 295(10):1255–1342

Rafalsky RP (1973) Hydrothermal equilibria and processes of minerals formation. Nauka, Moscow, 288 p. Free book site: http://www.geokniga.org/books/7820 (in Russian)

Red'kin AF (2000) Experimental study of the behavior of ore-forming compounds in the system WO_3–SnO_2–UO_2–NaCl–H_2O at 400–500 °C, 200–1000 bar and the hematite-magnetite buffer. Geochem Int 38(Suppl. 2):S227–S236

Redkin AF (1983) Experimental and thermodynamical investigation of frontier reactions controlling conditions of formation of wall-rock beresites. Thesis of Ph.D., Vernadsky Institute of RAS, Moscow, 27 p (in Russian)

Redkin AF, Kostromin NP (2010) On the problem of transport species of tungsten by hydrothermal solutions. Geochem Int 48(10):988–998

Redkin AF, Savelyeva NI, Sergeyeva EI, Omelyanenko BI, Ivanov IP, Khodakovsky IL (1989) Investigation of uraninite (UO_2) solubility under hydrothermal conditions. Strasbourg Sci Geol Bull 42(4):329–334

Redkin AF, Zaraisky GP, Velichkin VI (1999) An influence of the phase conversions in water-salt systems and rock-buffered action on solubility and partitioning of some ore elements (W, Sn, U). In: Abstracts: international symposium "physico-chemical aspects of endogenic geological processes" devoted to the 100-anniversary of D.S. Korzhinskii. Moscow, Russia, pp 182–183

Redkin AF, Kotova NP, Shapovalov YB (2015) Liquid immiscibility in the system NaF–H_2O at 800 °C and 200–230 MPa and its effect on the microlite solubility. J Sol Chem 44(10):2008–2026

Robie RA, Hemingway BS (1995) Thermodynamic properties of minerals and related substances at 298.15 K and 1 bar (105 pascals) pressure and at higher temperatures. US Geol Surv Bull 2131:461 p

Robie RA, Hemingway BS, Fisher JR (1978) Thermodynamic properties of minerals and related substances at 298.15 K and 1 bar (10^5 pascals) pressure and at higher temperatures. US Geol Surv Bull 1452:456 p

Ryzhenko BN (1981) Thermodynamics of equilibria in hydrothermal conditions. Nauka, Moscow, 191 p

Shmulovich KI, Tkachenko SI, Plyasunova NV (1995) Phase equilibria in fluid systems at high pressures and temperatures. In: Shmulovich KI, Yardley BWD, Gonchar GG (eds) Fluids in the crust: equilibrium and transport properties. Chapman and Hall, London, pp 193–214

Shock EL, Sassani DC, Willis M, Sverjensky DA (1997) Inorganic species in geologic fluids: correlations among standard molal thermodynamic properties of aqueous ions and hydroxide complexes. Geochim Cosmochim Acta 61:907–950

Shvarov YuV (2008) HCh: new potentialities for the thermodynamic simulation of geochemical systems offered by Windows. Geochem Int 46(8):834–839

Shvarov Yu (2015) A suite of programs, OptimA, OptimB, OptimC, and OptimS compatible with the Unitherm database, for deriving the thermodynamic properties of aqueous species from solubility, potentiometry and spectroscopy measurements. Appl Geochem 55:17–27

Shvarov YuV, Bastrakov E (1999) HCh: a software package for geochemical equilibrium modeling. User's guide 3.3. Australian Geological Survey Organization, 25 p

Smirnov VI, Ginsburg AI, Grigoriev VM, Yakovlev GF (1981) Course of ore deposits. High school manual. Nedra Press, Moscow, pp 161–174 (348 p) (in Russian)

Tagirov BR (1998) Experimental and computational study of the form iron transport in chloride hydrothermal solutions. Ph.D. thesis, IGEM RAN, Moscow, 22 p (in Russian)

Teleshova RL (1973) Differential spectrophotometric micromethod for silica determination in silicate minerals and rocks. Nauka Press, Moscow, pp 26–29 (in Russian)

Veispäls A (1979) Thermodynamic investigations of the chemical transport of tungsten trioxide. Izv Latv Acad Sci Seriya Phys Tech Sci 1:60–65 (in Russian)

Volina OV, Barabanov VF (1995) To the concern of tungsten existence forms in hydrothermal solutions. Proc Russ Mineral Soc 4:1–11 (in Russian)

Wesolowski D, Drummond SE, Mesmer RE, Ohmoto H (1984) Hydrolysis equilibria of tungsten(VI) in aqueous sodium chloride solutions to 300 °C. Inorg Chem 23:1120–1132

Wood SA, Samson IM (2000) The hydrothermal geochemistry of tungsten in granitoid environments: I. Relative solubility's of ferberite and scheelite as a function of T, P, pH, and mNaCl. Econ Geol 95:143–182

Wood SA, Vlassopoulos D (1989) Experimental determination of the hydrothermal solubility and speciation of tungsten at 500 °C and 1 kbar. Geochim Cosmochim Acta 53:303–312

Zaraisky GP (1995) The influence of acidic fluoride and chloride solutions on the geochemical behavior of Al, Si and W. In: Shmulovich KI, Yardley BWD, Gonchar GG (eds) Fluids in the crust: equilibrium and transport properties. Chapman and Hall, London, pp 139–162